Infrared absorption on a complex comprising three equivalent hydrogen atoms in ZnO

F. Herklotz,* A. Hupfer, K. M. Johansen, and B. G. Svensson
University of Oslo, Department of Physics, Centre for Materials Science and Nanotechnology, P.O. Box 1048, Blindern, N-0316 Oslo, Norway

S. G. Koch and E. V. Lavrov
Technische Universität Dresden, D-01062 Dresden, Germany
(Received 21 June 2015; published 9 October 2015)

A hydrogen-related defect in ZnO which causes two broad IR absorption bands at 3303 and 3321 cm^{-1} is studied by means of infrared absorption spectroscopy and first-principles theory. In deuterated samples, the defect reveals two sharp absorption lines at 2466 and 2488 cm^{-1} accompanied by weaker sidebands at 2462 and 2480 cm^{-1}. Isotope substitution experiments with varying concentrations of H and D together with polarization-sensitive measurements strongly suggest that these IR absorption lines are due to stretch local vibrational modes of a defect comprising *three* equivalent hydrogen atoms. The zinc vacancy decorated by three hydrogen atoms, $V_{Zn}H_3$, and ammonia trapped at the zinc vacancy, $(NH_3)_{Zn}$, are discussed as a possible origin for the complex.

DOI: 10.1103/PhysRevB.92.155203 PACS number(s): 61.72.jd, 78.30.Fs

I. INTRODUCTION

Hydrogen (H) in semiconductors is fascinating to study and this holds especially for zinc oxide (ZnO) where it is a prevailing impurity of fundamental importance. In ZnO, H strongly influences the electrical and optical properties, either by (i) introducing shallow donor states in, e.g., H_i or H_O configuration [1–3], or (ii) passivating residual acceptors. In fact, the presence of H and its interaction with intrinsic point defects and other impurities may hold a basic key to the eluding *p*-type conductivity of ZnO by extrinsic (as well as intrinsic) acceptor doping.

The microscopic structure of several acceptor-hydrogen complexes is well established [4–9], whereas the nature of many hydrogen-related defects remains unclear. In a recent IR absorption study, Parmar *et al.* [10] attributed a relatively broad transition at $\sim$3303 cm^{-1} to the O-H stretching mode of the Na acceptor passivated by a single hydrogen atom. Notably, the IR absorption spectra were recorded with the incident light perpendicular to the surface of the *c*-cut ZnO samples. In this configuration, however, local vibrational modes (LVMs) with transition dipole moment parallel to the *c* axis of the crystal are not detectable. In several other works, the LVM at 3303 cm^{-1} was observed together with a second broad mode at $\sim$3321 cm^{-1} [6,8,11]. However, a detailed investigation of the complex giving rise to these modes has not been reported in the literature so far.

Here, we present the results of a combined infrared absorption and first-principles theory study on single-crystalline ZnO, which rule out the assignment of the 3303 cm^{-1} line to the Na-related defect. Our isotopic substitution experiments and polarization-sensitive measurements show that the two absorption lines at 3303 and 3321 cm^{-1} should be attributed to the twofold-degenerate asymmetric and single-degenerate symmetric stretch modes of a defect consisting of three equivalent hydrogen atoms, respectively. The zinc vacancy decorated with three hydrogen atoms, $V_{Zn}H_3$, and ammonia trapped at the zinc vacancy, $(NH_3)_{Zn}$, are considered as possible candidates for the center.

II. EXPERIMENTAL AND COMPUTATIONAL DETAILS

Two types of ZnO crystals have been used in this study. Hydrothermally grown (HT) ZnO substrates were purchased from three different suppliers (Tokyo Denpa Co., Ltd, SPC Goodwill, and Crystec GmbH) and *m*- or *c*-face cut with a size of $5 \times 5 \times 0.5$ mm^3. The second type was nominally undoped material grown from the vapor phase (VP) at the Institute for Applied Physics, University Erlangen (Germany). The samples were hexagonal prisms with a thickness of $\sim$2 mm and a length of $\sim$20 mm. Hydrogen or/and deuterium was/were introduced into the samples via thermal treatments in sealed quartz ampoules filled with hydrogen or/and deuterium gas (pressure of 0.5 bar at room temperature). The treatments (hydrogenations) were performed in the temperature range 560–1000 °C for 1 h and were terminated by quenching to room temperature in water.

Generally, this procedure results in a strong broad IR absorption due to the free carriers introduced into ZnO via formation of shallow donor states. In order to suppress the free carrier absorption and facilitate the investigation of the defect of interest, the samples have been subsequently heat treated (annealed) in the temperature range 200–500 °C. The annealings were performed in a tube furnace in air ambient for 30 min and terminated by a cooldown to room temperature within about 2 min. The thermal stability of IR absorption lines was studied in a series of annealings in the temperature range 50–850 °C.

Fourier transform infrared (FTIR) absorbance spectra were recorded with a Bruker IFS125 HR spectrometer equipped with a globar light source, a CaF_2 beam splitter, and an InSb detector. Unless noted otherwise, the measurements were performed at 16 K with a spectral resolution of 0.5 cm^{-1}. Unless stated otherwise, unpolarized light was used with the wave vector, $\boldsymbol{k}$, directed perpendicular to the *c* axis of the samples. Polarized light was produced by a wire-grid polarizer with KRS-5 substrate.

*frank.herklotz@smn.uio.no

Density functional theory (DFT) calculations were performed using the plane-wave projector augmented-wave method [12] with the Perdew-Burke-Ernzerhof (PBE) generalized gradient approximation functional [13] as implemented in the VASP code [14]. The initial geometries were set up using molecular dynamics with 1 fs time steps for 5 ps in a 1000 K bath followed by quenching to 0 K over 10 ps. The geometries were then relaxed until the Feynman-Hellmann forces were below 50 meV/Å. The binding energies were calculated using 192 atom supercells with a 400 eV cutoff energy and eight k points. For vibrational calculations 72 atom supercells were used and an increased cutoff energy of 450 eV yielded converged vibrational energies using linear response theory as implemented in VASP. Vibrational dipole directions were determined using a method similar to Karhanek *et al.* [15].

III. RESULTS

A. General properties of the IR lines

Figure 1 shows sections of IR absorbance spectra for hydrothermally grown ZnO samples after thermal treatments at 715 °C in H_2, D_2, and $H_2 + D_2$ ambient and subsequent annealing at 400 °C. Two broad absorption features at ∼3303 and ∼3321 cm^{-1} are seen in the hydrogen-treated sample (top spectrum). The intensity ratio of the 3303 and 3321 cm^{-1} signals is independent of the sample indicating the same origin of the defect. Throughout this work we will label it XH_3, whereas its IR absorption lines at 3303 and 3321 cm^{-1} will be denoted as σ_1^H and σ_2^H, respectively.

When hydrogen is substituted by deuterium (mid spectrum), absorption peaks appear in the frequency range 2462–2488 cm^{-1}. The frequency ratio of the hydrogen- and deuterium-related lines is ∼1.34, which is close to $\sqrt{2}$—the value expected for a harmonic oscillator consisting of hydrogen bound to some not yet identified atom X. Later on we will show that the most probable candidates for X are the host oxygen atom and nitrogen.

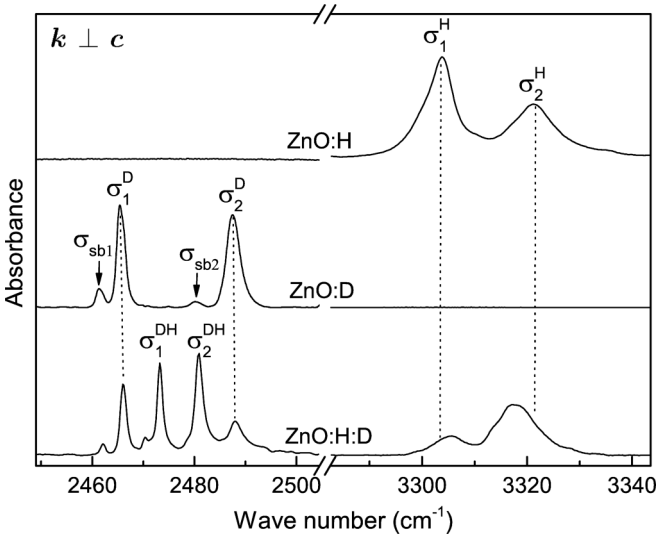

FIG. 1. Normalized IR absorbance spectra of HT ZnO samples after thermal treatments in H_2, D_2, and $H_2 + D_2$ ambient at 725 °C and subsequent annealing at 400 °C for 30 min in air.

As follows from the figure, two main modes at 2466 cm^{-1} (σ_1^D) and 2488 cm^{-1} (σ_2^D) are observed in the spectrum of the deuterium-treated sample. Furthermore, two sidebands at 2462 cm^{-1} (σ_{sb1}) and 2480 cm^{-1} (σ_{sb2}) can be clearly resolved in the spectrum. Interestingly, all deuterium-related absorption lines are significantly sharper than its hydrogen-related counterparts.

If the sample is treated with hydrogen and deuterium (bottom spectrum), two additional main modes at 2473 cm^{-1} (σ_1^{DH}) and 2480 cm^{-1} (σ_2^{DH}) and a mode of minor intensity at 2471 cm^{-1} are observed in the deuterium-related region of the spectrum. Note that also a sideband at 2479 cm^{-1} arises, which appears in Fig. 1 as a weak shoulder of the main mode at 2480 cm^{-1}, but is clearly resolved in other spectra of this work (see, for instance, Fig. 5). The isotopically mixed XH_3 center also results in additional hydrogen-related modes positioned between σ_1^H and σ_2^H. At this stage substantial broadening of the lines prevents us from drawing solid conclusions on the number and frequency of these "mixed" LVMs. The results which will be presented later on will, however, reveal much clearer information.

We note that the IR spectra of samples presented in Fig. 1 are dominated by absorption lines at 3577 and/or 2644 cm^{-1} (not shown), which are due to the O-H and/or O-D stretch vibration(s) of the OH-Li_{Zn} center [7–9]. Some of our ZnO crystals, however, reveal weak hydrogen-related absorption lines outside the regions presented in the figure. The frequency and intensity of these transitions varied from sample to sample. Based on the entirety of our data, we conclude that only the absorption lines shown in Fig. 1 can be attributed to the XH_3 center.

Figure 2 shows IR absorption spectra of HT-grown ZnO samples after hydrogenation at 715 °C and subsequent annealing at 400 °C. The spectra are normalized to the integrated absorption in the range 2460–2495 cm^{-1}. The bottom

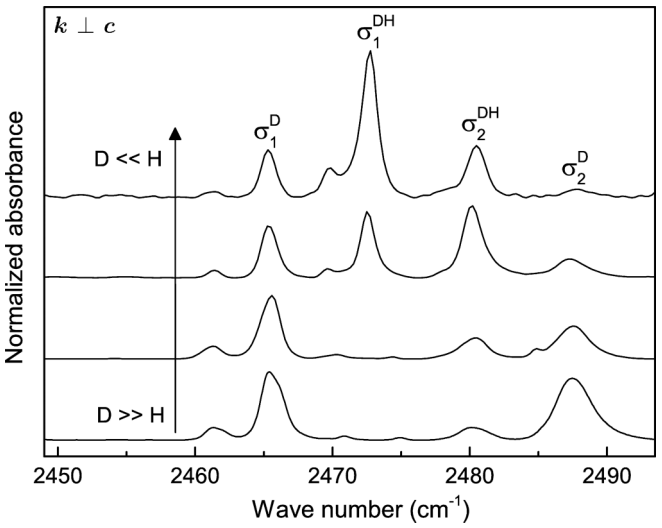

FIG. 2. IR absorption spectra of HT-grown ZnO samples hydrogenated at 715 °C in the $H_2 + D_2$ ambient with different concentration ratios [H]/[D] and subsequently annealed at 400 °C. The spectra are normalized to the integrated absorption in the range 2460–2495 cm^{-1}.

spectrum was recorded for a sample that had been treated in D_2 gas alone, whereas the samples of the three upper spectra were treated in a mixture of $H_2 + D_2$ with increasing H_2:D_2 ratio. From the bottom to the top spectrum, the relative hydrogen concentrations $r = [H]/([H] + [D])$ are 0.02, 0.22, 0.48, and 0.7, respectively [16]. As unveiled by the figure, the relative intensities of deuterium-related LVMs depend on r. With increasing hydrogen content ($r \to 1$), the "mixed" modes σ_1^{DH} and σ_2^{DH} gain intensity at the expense of the "pure" deuterium-related LVMs σ_1^{D} and σ_2^{D}. Interestingly, the relative intensity of σ_1^{D} and σ_2^{D} turned out to be a function of r: for $r \to 1$ the σ_1^{D} mode dominates over σ_2^{D}. Moreover, the "mixed" LVM σ_1^{DH} is marginal compared to σ_2^{DH} for $r \to 0$, but becomes dominant as $r \to 1$. A detailed discussion of this behavior will be presented in Sec. IV A.

B. Formation and thermal stability of the XH_3 center

Figure 3 shows the results of two isochronal annealing series that were obtained for an as-received HT-grown sample and a HT-grown sample after hydrogenation in H_2 gas at 715 °C, respectively. The data represent normalized integrated LVM intensities of the XH_3 center.

In the case of the sample treated in H_2 gas, the signals of the XH_3 center remain constant up to ∼500 °C and anneal out at 750 °C. A similar thermal behavior is observed for the deuterium counterparts, if the sample is treated in D_2 gas (not shown). In contrast, the XH_3 center is not observed in as-received samples for annealing up to ∼250 °C. As the temperature is raised further, the intensity of the XH_3 absorption lines gradually increases up to a maximum at ∼ 500 °C. Finally, at higher temperatures, the thermal behavior is similar to that of a sample treated in H_2 gas. Notably, the relative intensity of all LVMs is found to be independent of the annealing temperature. This result confirms our previous conclusion that the IR lines originate from the same defect.

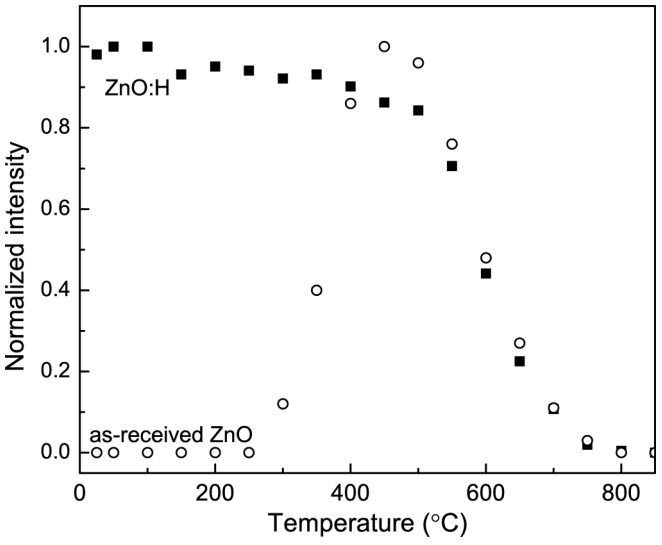

FIG. 3. Normalized intensities of the IR absorption lines due to the XH_3 center as a function of the temperature in an isochronal annealing series. ○, as-received HT-grown ZnO; ■, HT-grown ZnO after treatment in H_2 gas at 715 °C.

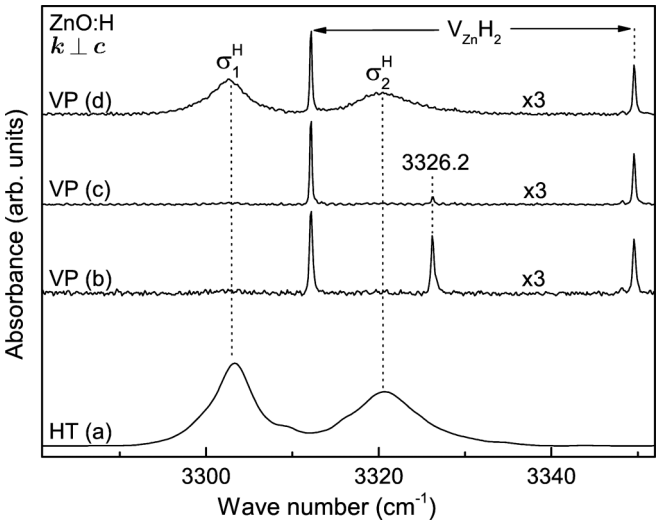

FIG. 4. IR absorption spectra of hydrothermally and vapor-phase-grown ZnO samples after hydrogenation at (a) 725 °C and subsequent annealing at 200 °C; (b) 725 °C; (c) 725 °C and subsequent annealing at 200 °C; and (d) 1000 °C and subsequent annealing at 200 °C.

So far, the XH_3 center was probed in hydrothermally grown ZnO. We want now to compare hydrothermally vs vapor-phase-grown crystals. Figure 4 shows absorbance spectra obtained from a series of treatments on both types of samples. Spectrum (a) is recorded on a HT-grown ZnO after introduction of H at 725 °C and a subsequent annealing at 200 °C. The XH_3 center is clearly evidenced by the σ_1^{H} and σ_2^{H} LVMs at 3303 and 3321 cm^{-1}, respectively. On the contrary, hydrogenation at 725 °C does not induce XH_3 centers in the VP-grown samples, but results in the formation of zinc vacancies passivated by two hydrogen atoms, $V_{Zn}H_2$ [5,11], and a defect, which causes a LVM at 3326.2 cm^{-1} [see spectrum (b)] [17,18]. The 3326 cm^{-1} line disappears after annealing at 200 °C [spectrum (c)], which is in agreement with a previous IR absorption study on this defect [18]. Finally, spectrum (d) was taken after hydrogenation of a VP-grown sample at 1000 °C followed by an annealing at 200 °C. This sample treatment results in the appearance of the LVMs at 3303 and 3321 cm^{-1}; however, the intensities of these lines are still significantly weaker than those obtained from the HT-grown sample.

C. Polarization dependence

Figure 5 shows polarized IR absorption spectra of a sample treated in a mixture of H_2 and D_2 gas and subsequently annealed at 400 °C. The σ_1^{D} line at 2466 cm^{-1} is fully polarized perpendicular to the c axis, whereas the σ_2^{D} line at 2488 cm^{-1} is fully polarized with the c axis. Thus, the transition dipole moments responsible for the σ_1^{D} and σ_2^{D} modes are perpendicular and parallel to c, respectively. On the contrary, the dipole moment of the mixed modes σ_1^{DH} and σ_2^{DH} deviates from an orientation perpendicular or parallel to the c axis of the crystal. From our polarized spectra, we can further conclude that the sidebands at 2462, 2471, and 2480 cm^{-1} are polarized perpendicular to c.

Figure 6 presents the normalized intensities of the LVMs at 2466, 2473, 2480, and 2488 cm^{-1} as a function of the polarizer

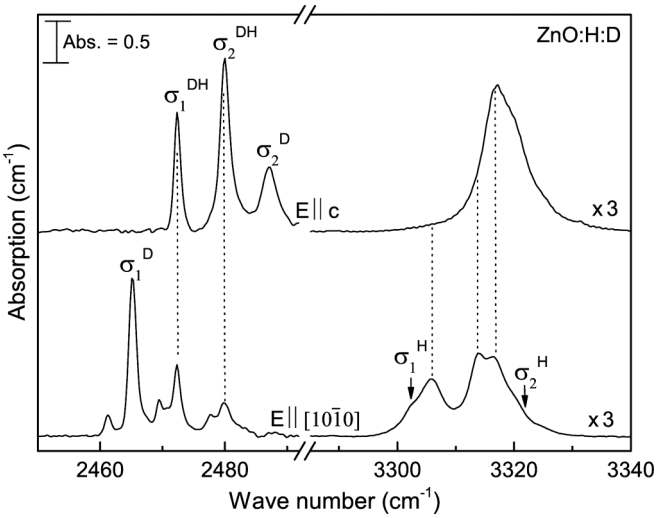

FIG. 5. Polarized IR absorption spectra of HT-grown ZnO treated in a mixture of H_2 and D_2 gas at 715 °C and subsequently annealed at 400 °C. The relative H concentration $r = [H]/([H] + [D])$ of this particular sample is 0.50.

orientation. Generally, the intensity of light absorbed by an electrical dipole vibrating in a crystal can be written as

$$I \propto \sum_{R_k} |\boldsymbol{e} \cdot (R_k \boldsymbol{d})|^2, \tag{1}$$

where $\boldsymbol{e}$ is the polarization vector of the light, $\boldsymbol{d}$ is the transition dipole moment, and R_k is the symmetry operator of the point group. For the C_{3v} symmetry of wurtzite ZnO, the deviation angle α of the transition dipole moment from the c axis can then be obtained from the ratio of the perpendicular-to-parallel intensities by

$$\alpha = \arctan\sqrt{2I_\perp/I_\parallel}. \tag{2}$$

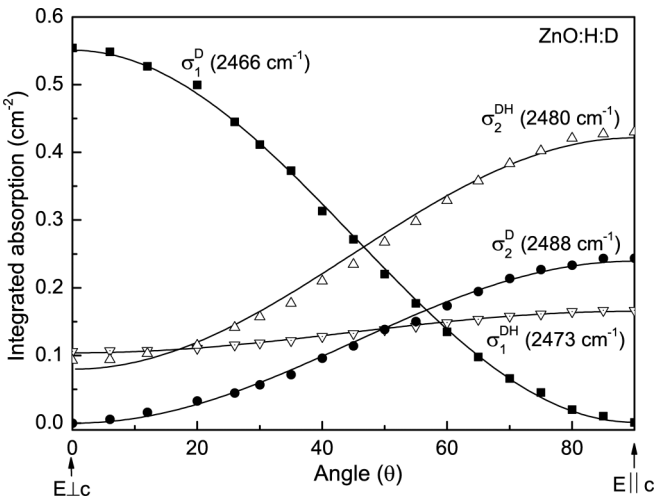

FIG. 6. Normalized LVM intensities of the XH_3 defect measured as a function of the angle θ between the polarizer and the c axis of the sample. Solid lines are best fits to Eq. (1).

From our polarization-dependent measurements and Eq. (2) we get the following values: $\alpha_{2466} = (86 \pm 4)$ °, $\alpha_{2473} = (48 \pm 3)$ °, $\alpha_{2480} = (32 \pm 5)$ °, and $\alpha_{2488} = (4 \pm 5)$ °.

Due to the substantial broadening of the lines, the orientation of the transition dipole moment for the hydrogen-related vibrational modes can only be determined to a much lower accuracy. Measurements on a sample treated in H_2 gas alone (not shown) revealed that the polarized behavior of σ_1^H and σ_2^H is equivalent to their deuterium-related counterparts.

D. Temperature dependence of the LVMs

Figure 7 shows the frequency shift (top) and full width at half maximum (FWHM) (bottom) of the local modes of XH_3 as a function of the temperature. The left panels present the data obtained for the σ_1^H and σ_2^H modes, whereas the right panels show those for the deuterium-related LVMs. The qualitative behavior of the frequency shift varies with the mode: The high-frequency LVMs σ_2^H (3321 cm^{-1}) and σ_2^D (2488 cm^{-1}) shift downwards with the temperature, whereas the low-frequency ones σ_1^H (3303 cm^{-1}) and σ_1^D (2466 cm^{-1}) move in the opposite direction. Consequently, the splitting between σ_2^H (σ_2^D) and σ_1^H (σ_2^D) decreases when the temperature rises. Interestingly, the mixed modes σ_1^{DH} (2473 cm^{-1}) and σ_2^{DH} (2480 cm^{-1}) experience a frequency shift $\Delta\omega = \omega - \omega_0$

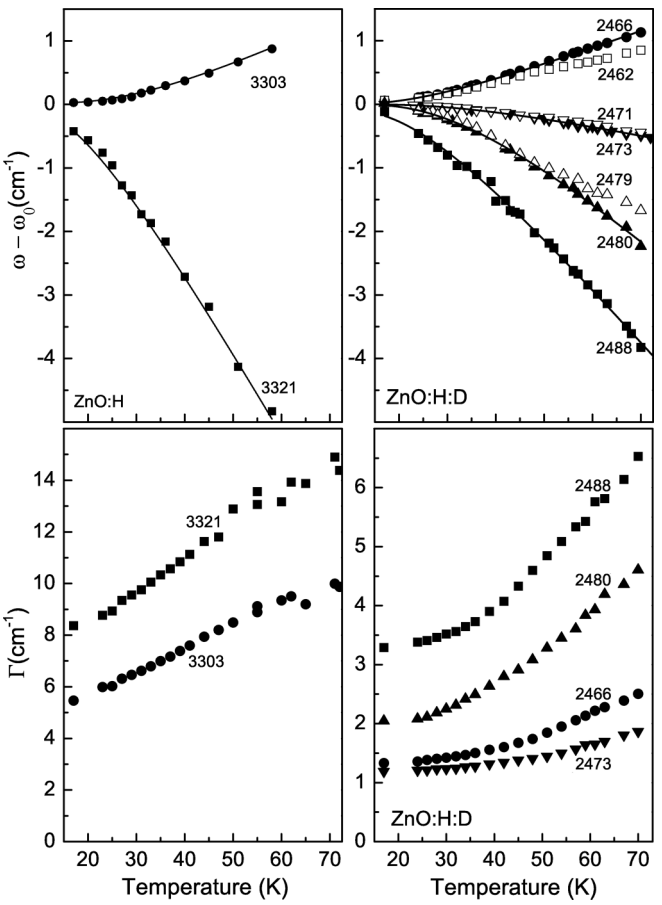

FIG. 7. Frequency shift and FWHM of XH_3 LVMs for a HT ZnO sample treated in H_2 gas (left panel) and a sample treated in a gas mixture of H_2 and D_2 (right panel). Solid lines are fits to Eq. (3).

that is midway compared to the pure deuterium-related modes, that is, $\Delta\omega_{2466} > 0 > \Delta\omega_{2473} > \Delta\omega_{2480} > \Delta\omega_{2488}$. Figure 7 also presents the values of $\Delta\omega$ for the three sideband transitions at 2462, 2471, and 2479 cm^{-1} (see Sec. III A). The temperature behavior of these modes closely follows that of their associated "main" modes σ_1^D, σ_1^{DH}, and σ_2^{DH}.

The temperature shift and broadening of LVMs have often been explained by a dephasing due to an anharmonic interaction with lattice vibrations, pseudolocalized modes, or other vibrational transitions. In the theory developed by Persson and Rydberg [19], the LVM couples to a single low-energy exchange mode through a parameter $\delta\omega$, which in turn interacts with the lattice vibrations through the "friction" parameter η. In the limit of small coupling $\delta\omega \ll \eta$, the temperature shift and width of the LVMs are then expressed by

$$\omega = \omega_0 + \frac{\delta\omega}{\exp(E_0/k_BT) - 1},$$
$$\Gamma = \frac{2(\delta\omega)^2}{\eta}\left(\frac{1}{2} + \frac{1}{\exp(E_0/k_BT) - 1}\right)^2. \quad (3)$$

This approach have been successfully used to model the behavior of several hydrogen-related stretch modes in ZnO (see, e.g., Refs. [6,11,18,20]). In order to explain the temperature dependence of the O-H stretch mode associated with the OH-Li_{Zn} complex in ZnO, Martin *et al.* extended the model of Persson and Rydberg to a coupling of the LVM to more than one exchange mode [21]. The energy of the exchange mode E_0 obtained in these works is in the range 51–103 cm^{-1}, which indicates that the modes are coupled to lattice vibrations rather than to bend modes or other stretch modes (see Ref. [21], and references therein). Notably, the values of E_0 have been also found to be independent of the isotopic defect configuration, that is, O-H and O-D stretch modes of the same defect couple to the same exchange mode.

The model by Persson and Rydberg [19] or Martin *et al.* [21] cannot, however, fully explain our experimental data on the stretch modes of XH_3. While the frequency shifts follow the exponential relation given in Eq. (3) reasonably well (see the corresponding fitting curves in Fig. 7), the low-temperature FWHM values are significantly higher then predicted. In particular, the FWHM of the σ_1^H (the 3303 cm^{-1} line), σ_2^H (3321 cm^{-1}), and σ_1^D (2488 cm^{-1}) modes are not in accordance with the model of Persson and Rydberg. Further, for these lines the above-mentioned weak-coupling condition $\delta\omega \ll \eta$ is not fulfilled.

Our results suggest that other contributions than anharmonic coupling to an exchange mode add to the resulting linewidth Γ of the LVMs of the XH_3 center. One possibility could be inhomogeneous line broadening mechanisms. Usually, the most important contribution to such processes for LVMs in semiconductors is due to strain fields induced by lattice defects. However, we found that the FWHM of the XH_3 modes are rather independent of the defect concentration. Furthermore, this mechanism does not give an intuitive explanation of the isotopic dependence of the linewidth. The broadening of vibrational modes can also be governed by processes that decrease the lifetime of the first-excited vibrational state. One of these processes is multiphonon decay, which has been suggested as the dominant relaxation channel for several LVMs in, e.g., Si, Ge, or GaAs [22]. The decay of the 3303 or 3321 cm^{-1} mode would, however, require at least five phonons of ZnO. This is not in agreement with the high FWHM $\Gamma > 5.2 cm^{-1}$ of these transitions, which correspond to a lifetime $T_1 = 1/(2\pi c\Gamma)$ shorter than 1 ps. In principle, the vibrational lifetime of the LVMs can also be influenced by proton transfer steps, as for instance suggested for the interstitial hydrogen in $KTaO_3$ [23] or TiO_2 [24]. Other potential explanations are resonances with other (pseudo-) LVMs [25,26] or decay into electronic degrees of freedom. One possibility to verify the nature of the line broadening is measurements of the vibrational lifetimes by pump-probe experiments. At the present stage, our experimental data do not permit one to draw a final conclusion.

IV. DISCUSSION

A. Microscopic structure

Parmar *et al.* [10] attributed the IR lines at 3303, 2466, and 2462 cm^{-1} to LVMs of sodium acceptors passivated by a single hydrogen. In their study, the absorption measurements were performed with the incident light beam parallel to the c axis of the ZnO crystals. However, in this geometry the modes at 3321 and 2488 cm^{-1} cannot be detected. Furthermore, hydrogenation was performed either from the pure hydrogen or pure deuterium ambient and, thus, modes from the isotopically mixed defect were not observed. On the other hand, our isotope substitution experiments together with polarization data unambiguously show that the XH_3 center contains more than one hydrogen atom which rules out the assignment by Parmar *et al.*

It is a nontrivial task to determine the exact number and configuration of hydrogen atoms in the XH_3 center. In particular because hydrogen-related modes are broad and represent a superposition of more than one LVM. However, symmetry of ZnO, the isotope substitution data, and polarization-dependent measurements significantly constrain the number of possible microscopic configurations of the defect. Because of the substantial broadening of the hydrogen-related lines, the following discussion will mainly focus on the results obtained for the deuterium siblings of XH_3 without, however, a loss of generality.

The experimental observations indicate that XH_3 consists of at least two hydrogen atoms. A structure with two equivalent hydrogen atoms can be excluded since in this case not more than one additional mode would be detected in the "mixed complex" case for both the hydrogen- and deuterium-related spectral region. The measurements presented in Sec. III C reveal that the polarization properties of the pure σ_1^D and σ_2^D modes are distinctively different from the mixed ones σ_1^{DH} and σ_2^{DH}. For a defect with two inequivalent hydrogen atoms this would imply that the coupling between them is so strong that substitution of one deuterium atom by hydrogen leads to a significant structural relaxation of the defect. Moreover, the experimental data indicate that the relative intensity of pure modes σ_1^D and σ_2^D as well as that of the mixed modes σ_1^{DH} and σ_2^{DH} differently depend on the isotope ratio. In our opinion,

TABLE I. Summary of results obtained for the LVMs of the XH_3 center. The temperature shift is defined as $\Delta\omega$ in Sec. III D. See text for details of the fit parameters a to e and ε.

Config.			Freq. (cm^{-1})	$I_\perp/I_\parallel$	T shift	Fit parameters
HHH	σ_2^{H}	A_1	3321	0	−	$\varepsilon e = 1.56$
	σ_1^{H}	E	3303	∞	+	$\varepsilon a = 1.37$
	σ_3^{HD}	A'	3318	0.24	−	$\varepsilon d = 1.45$
HHD	σ_1^{HD}	A''	3305	∞	+	$\varepsilon b = 0.66$
	σ_1^{DH}	A'	2473	0.62	−	$c = 0.96$
	σ_2^{HD}	A'	3314	0.67	−	$\varepsilon c = 1.32$
HDD	σ_2^{DH}	A'	2480	0.18	−	$d = 1.06$
	(σ_1^{D})	A''	2466	∞	+	$b = 0.48$
DDD	σ_2^{D}	A_1	2488	0	−	$e = 1.16$
	σ_1^{D}	E	2466	∞	+	$a = 1$

these findings cannot be explained by a complex that contains two inequivalent hydrogen atoms either.

For the "isotopically pure" XH_3 center, two major stretch modes are observed with transition dipole moments either parallel or perpendicular to the c axis. A defect with three equivalent hydrogen atoms can account for these findings. The assignments of all LVMs of the defect following this model are given in Table I. The σ_1^{H} (or σ_1^{D}) stretch mode would then stand for the twofold degenerate E representation of the C_{3v} point group, whereas σ_2^{H} (or σ_2^{D}) would represent the symmetric A_1 one. This model also naturally explains properties of the combinational LVMs. The σ_1^{DH} mode should belong to the XH_3 complex with one deuterium and two hydrogen atoms, whereas σ_2^{DH} is a symmetric stretch mode of XH_3 with two deuterium and one hydrogen atoms. The asymmetric stretch mode of this configuration overlaps with the σ_1^{D} mode of the isotopically pure center at 2466 cm^{-1} and cannot be resolved as a separate absorption feature in the spectra. In Table I, we therefore label the asymmetric stretch mode as (σ_1^{D}). Contrary to the deuterium case, the mixed σ_1^{HD} and the pure σ_1^{H} modes for the hydrogen-related counterparts are separated by ∼2 cm^{-1}. The isotopically-mixed defect thus leads to three separated hydrogen-related modes σ_1^{HD}, σ_2^{HD}, and σ_3^{HD} at 3305, 3314, and 3318 cm^{-1}, respectively, as can be seen, for instance, by the dotted lines in Fig. 5.

Now we want to verify if the results of the isotope substitution experiments are consistent with our model of the defect. We expect that if hydrogen is substituted by deuterium isotopes, the combinational modes will appear in the spectra at the expense of the "pure" ones. Since the concentration of XH_3 depends on the treatment conditions, the absolute intensity of these LVMs will vary from sample to sample. However, the relative intensities will be solely a function of the isotopic ratio $r = [H]/([H] + [D])$. In assumption that the incorporation of hydrogen and deuterium on a certain position in the XH_3 center is governed by statistics, the probability for the formation of a defect with at least one deuterium atom will be proportional to $(1 - r)^3$ (three deuterium atoms), $r(1 - r)^2$ (one hydrogen and two deuterium atoms), and $r^2(1 - r)$ (two hydrogen and one deuterium atom). The intensity of the LVMs is then

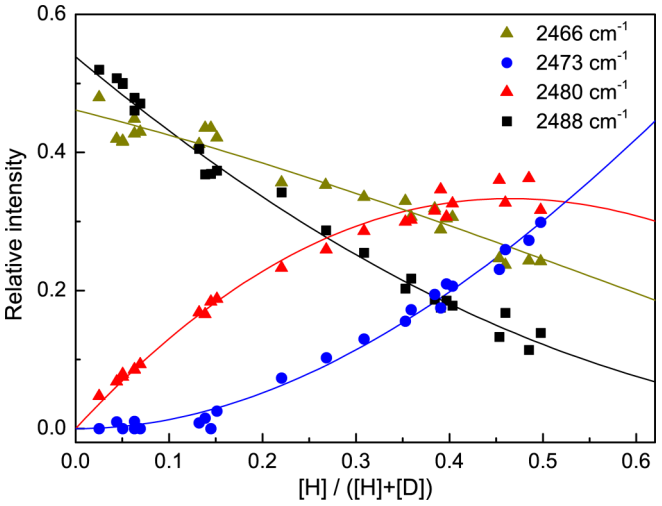

FIG. 8. (Color online) Best fit of relative LVM intensities of the XH_3 center obtained from isotopic substitution experiments to the defect model described by Eq. (4) and consisting of three symmetry-equivalent hydrogen/deuterium atoms. The samples were hydrogenated by annealing in D_2 or $H_2 + D_2$ ambient with different H_2:D_2 ratios and at different temperatures in the temperature range 560–1000 °C. The relative H concentration $r = [H]/([H] + [D])$ is treated as a parameter and independently varied for each sample to give the best fit to all data. See text for more details of the fitting procedure.

given by

$$\begin{aligned} I_{2466} &= [a(1-r)^3 + br(1-r)^2][XH_3], \\ I_{2473} &= cr^2(1-r)[XH_3], \\ I_{2480} &= dr(1-r)^2[XH_3], \\ I_{2488} &= e(1-r)^3[XH_3], \end{aligned} \tag{4}$$

where a, b, c, d, and e are parameters, which represent the oscillator strength and degeneracy ratio of the specific LVMs. The relative intensity of these LVMs compared to the intensity $I_\sum = I_{2466} + I_{2473} + I_{2480} + I_{2488}$ is an observable which we can obtain from our measurements.

Figure 8 shows the relative intensities of the deuterium-related stretch modes of the XH_3 center together with the best-fit curves as a function of r obtained for 22 different hydrothermally and vapor-phase-grown ZnO samples. Since the value of r was not known *a priori*, it was also treated as a fitting parameter. As follows from the figure, our model accounts for the experimental data reasonably well. The best-fit values of a-e are given in Table I.

The consistency of the present model was verified by simulation of the intensities of the hydrogen-related modes for all samples presented in Fig. 8. Here, one has to assume that the absorption strength of the hydrogen-related LVMs is scaled up by a factor ε compared to the deuterium-related counterparts. Figure 9 shows the corresponding modes normalized to the total intensity of all deuterium-related modes of XH_3 with the corresponding calculated curves (solid lines). For the sake of clarity, the data are grouped up in the "low-frequency" σ_1^{H} and σ_1^{HD} (3303 and 3305 cm^{-1}), the "high-frequency" σ_2^{HD}, σ_3^{HD}, and σ_2^{H} (3312–3321 cm^{-1}), and the total sum of the

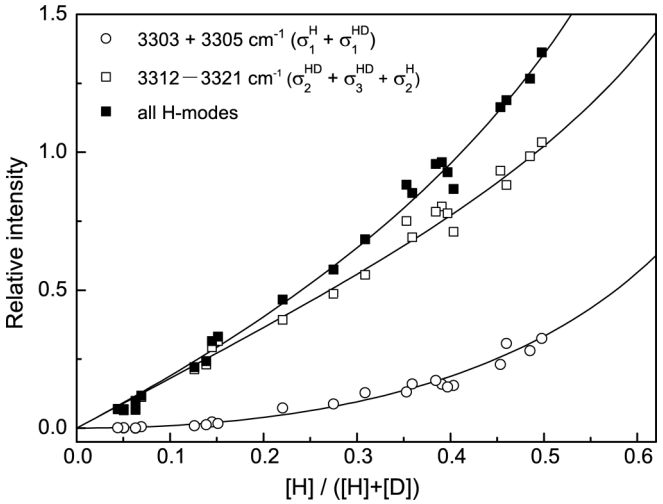

FIG. 9. Relative intensities of hydrogen modes of the $X\mathrm{H}_3$ center for the same samples as in Fig. 8. The intensities are normalized to the total integrated absorption of the deuterium-related LVMs of $X\mathrm{H}_3$. ○, sum of σ_1^{H} and σ_1^{HD}; □, sum of σ_3^{HD}, σ_3^{HD}, σ_2^{HD}, and σ_2^{H}; and ■, sum of all H-related mode intensities of $X\mathrm{H}_3$. Solid lines: calculated curves as described in the text.

hydrogen-related modes. The close agreement between the simulated curves and the experimental data provides strong support for our model of $X\mathrm{H}_3$. We also note that the best-fit value for ε is 1.37 ± 0.03, which matches the value expected for an ideal O-H (N-H) harmonic oscillator, $\sqrt{\mu_{\mathrm{D}}/\mu_{\mathrm{H}}} = 1.37$.

Regarding the polarization of the vibrational lines, we assume that the transition dipole moments $\boldsymbol{d}$ of the LVMs are linear combinations of the dipole moments of each X-H (X-D) bond ($\boldsymbol{d}_1$, $\boldsymbol{d}_2$, and $\boldsymbol{d}_3$) aligned are parallel to the bonds. It is further assumed that the coupling between each bond is sufficiently weak so that in an "isotopically mixed" $X\mathrm{H}_3$ center the vibrating X-H and X-D species are practically decoupled. Since σ_2^{DH} originates from the isotopic combination with one deuterium and two hydrogen atoms, the angle between as single X-D bond and the c axis can be immediately obtained from the polarization properties of the σ_1^{DH} mode (see Sec. III C), $\vartheta_{2473} = (48 \pm 3)^\circ$ [or $(23 \pm 3)^\circ$ deviation from the perfect tetrahedral configuration].

On the other hand, the σ_2^{DH} mode is assigned to the symmetric stretch mode of two X-D species in the isotopic combination with two deuterium atoms and one hydrogen atom. The dipole moment of this mode is given by $\boldsymbol{d}_s = (\boldsymbol{d}_1 + \boldsymbol{d}_2)/\sqrt{2}$. From the polarized spectra and Eq. (1), we obtain that the angle between the X-D bond and the c axis is $\vartheta_{2480} = (52 \pm 4)^\circ$ [or $(19 \pm 4)^\circ$ from the perfect tetrahedral configuration], which is in good agreement with the orientation ϑ_{2473} obtained for σ_1^{DH}. Hence, also the polarization properties of the X-D modes corroborate the validity of the proposed model. Note that ϑ_{2480} is slightly overestimated since the σ_2^{DH} mode at 2480 cm^{-1} overlaps with the weak sideband σ_{sb2}, which is fully polarized perpendicular to c.

B. Nature of the sidebands

Sideband transitions of hydrogen stretch modes have been observed for a number of defects in ZnO, such as Cu-H [27], $V_{\mathrm{Zn}}\mathrm{H}_2$ [5], or the defect resulting in a LVM at 3326 cm^{-1} [18]. The microscopic origin of the sidebands is not well established so far, though, possible mechanisms have been discussed in the literature (see, for instance, Ref. [27]). One of the possible explanations is a metastable off-axis orientation of the X-H bond, as has been observed, for example, for the VH defect in silicon [28]. The sidebands may then be attributed to the resulting splitting of the ground state energies. Unfortunately, the weak intensity and considerable FWHM do not enable proper investigation of the thermal activation of the sidebands for the $X\mathrm{H}_3$ complex.

The defect model of a center with three X-D bonds also suggests another explanation for the nature of the sidebands at 2462, 2473, and 2480 cm^{-1}: a metastable configuration of the center, in which one X-H bond is aligned parallel to c, whereas the other two are positioned perpendicular to the c axis. A similar situation is observed for the zinc vacancy passivated by two hydrogen atoms, $V_{\mathrm{Zn}}\mathrm{H}_2$. This complex has two structural configurations, which are only separated by an energy difference of 75 meV [11]. In the ground state, one of the O-H bonds is aligned parallel to the c axis and the second one is oriented almost perpendicular to c [5]. In the metastable state, $V_{\mathrm{Zn}}\mathrm{H}_2^*$, the defect comprises two equivalent O-H bonds located in the basal plane of ZnO [11].

With this assumption, the sidebands at 2462 and 2480 cm^{-1} of the metastable configuration, $X\mathrm{H}_3^*$, would then be the asymmetric and symmetric stretch modes of two equivalent X-D bonds, whereas the one at 2471 cm^{-1} would be related to the isotopically mixed center with one hydrogen and one deuterium atom in the basal plane. From our polarization-dependent measurements one obtains that the angle between the X-D bonds with the c axis in $X\mathrm{H}_3^*$ would be $\vartheta = (82 \pm 8)^\circ$ (or $(11 \pm 8)^\circ$ deviation from the perfect tetrahedral configuration).

A drawback of the model with different orientations of the X-H species is a missing mode of the X-D bond oriented parallel to the c axis which may be due to a weak intensity of this line or/and an overlapping with other transitions. At this stage we can neither conclusively support nor rule out the $X\mathrm{H}_3^*$ model.

A further possibility to verify the structural models of $X\mathrm{H}_3$ and $X\mathrm{H}_3^*$ are experiments on the uniaxial stress splitting of the LVMs. This would unambiguously reveal the symmetry of the centers and, in turn, give further insight into their microscopic structure. Furthermore, stress-induced dichroism of the IR absorption lines could unveil energy barriers between different configurations of the complex or for hydrogen jumps between different positions.

C. The NH_3 model

A model of NH_3 trapped at the Zn vacancy is proposed to explain the important experimental observation that the frequency difference between hydrogen-related modes $\Delta\sigma^{\mathrm{D}} = \sigma_2^{\mathrm{D}} - \sigma_1^{\mathrm{D}} = 24$ cm^{-1} is larger than $\Delta\sigma^{\mathrm{H}} = \sigma_2^{\mathrm{H}} - \sigma_1^{\mathrm{H}} = 18\ \mathrm{cm}^{-1}$. This situation is possible if all hydrogen atoms are bound to the same X species of which nitrogen seems to be the most plausible one (see, e.g., the case of $\mathrm{H}_2\mathrm{O}$ [29]).

Vibrational frequencies of $X\mathrm{H}_3$ can be obtained in the valence force approximation from the solution of the secular

TABLE II. Best-fit parameters of Eqs. (5)–(7) for the LVMs of XH_3.

Config.		Freq. Expt. (cm^{-1})	Freq. Model (cm^{-1})	Pol. angle Expt. (deg.)	Pol. angle Model (deg.)
HHH	σ_2^{H}	3321	3321	$\parallel c$	$\parallel c$
	σ_1^{H}	3303	3303	$\perp c$	$\perp c$
	σ_3^{HD}	3318	3315	–	34
HHD	σ_1^{HD}	3305	3303	–	$\perp c$
	σ_1^{DH}	2473	2473	48 ± 3	54
	σ_2^{HD}	3314	3309	–	54
HDD	σ_2^{DH}	2480	2480	32 ± 5	34
	(σ_1^{D})	2466	2466	$\perp c$	$\perp c$
DDD	σ_2^{D}	2488	2488	$\parallel c$	$\parallel c$
	σ_1^{D}	2466	2466	$\perp c$	$\perp c$
$f = 574.56$ N/m				$\vartheta = 88.55°$	
$n = 0.38$ N/m				$m_X = 7.65$ a.u.	

equation [30]

$$\|\hat{\boldsymbol{F}}\hat{\boldsymbol{G}} - \sigma^2\hat{\boldsymbol{E}}\| = 0, \tag{5}$$

with the identity matrix $\hat{\boldsymbol{E}}$ matrices and

$$\hat{\boldsymbol{F}} = \begin{pmatrix} f & n & n \\ n & f & n \\ n & n & f \end{pmatrix}, \tag{6}$$

$$\hat{\boldsymbol{G}} = \begin{pmatrix} 1/\mu & \cos\vartheta/m_X & \cos\vartheta/m_X \\ \cos\vartheta/m_X & 1/\mu & \cos\vartheta/m_X \\ \cos\vartheta/m_X & \cos\vartheta/m_X & 1/\mu \end{pmatrix}. \tag{7}$$

Here, f is the force constant of the X-H bond, n and ϑ are the interaction force constant and the $\sphericalangle$ H-X-H angle between two X-H bonds, respectively; $1/\mu = 1/m_X + 1/m_{H(D)}$ with $m_H = 1.008$ a.u., $m_D = 2.014$ a.u., and m_X is the mass of the central trap atom. Obviously, the results of the least-square fit presented in Table II are in good agreement with the experimental observations. An apparent problem of this fit is the value of $m_X \approx {}^7$Li because no correlation between the X-H complex and the lithium content in our samples was found. This contradiction can be solved if we assume that m_X is in fact a reduced mass of X bound to the host atom [31]. The best match to the value of 7.65 is obtained for the X-^{16}O or X-^{65}Zn species with ^{14}N or ^{9}Be as X.

Nitrogen is used as a carrier gas for the transport of hydrogen during the crystal growth [32]. Additionally, annealing in air above 700 °C facilitates the in-diffusion of nitrogen atoms [33]. Recent first-principles calculations in Ref. [34] reveal that under oxygen-rich conditions ammonia bound to oxygen in a zinc vacancy $(NH_3)_{Zn}$ is thermodynamically the most stable nitrogen-related complex in ZnO. This neutral defect can exist in two configurations: one with the N-O axis aligned parallel to the c axis and the other with N-O lying in the basal plane. These findings match the present experimental observations obtained for the XH_3 and XH_3^* complexes. Notice that the bond angle ϑ of ammonia in ZnO differs from that of the gaseous species $\vartheta_{gas} = 106.7$ ° (see Ref. [29]) due to local rearrangement of the molecule in the ZnO matrix.

Reference [34] does not give LVM frequencies of the $(NH_3)_{Zn}$ complex. We have calculated formation energies and vibrational frequencies for both configurations of $(NH_3)_{Zn}$. Similar to Ref. [34] and in agreement with the experiments we find that $(NH_3)_{Zn}$ is stable, where the complex with the N-O axis aligned parallel to the c axis is energetically more favorable than with N-O lying in the basal plane. However, our calculations reveal that the H-related LVM frequencies for both configurations of the complex are in the range 2100–2500 cm^{-1}, considerably lower than that observed in our experiments. The hydrogen atoms in $(NH_3)_{Zn}$ are primarily bound to nitrogen, however, the N-H vibrational frequencies are significantly redshifted compared to the free N-H bond due to the nearby oxygen atoms, which stretches the hydrogen atoms away from the nitrogen. This is evident by typical N-H bond lengths for both $(NH_3)_{Zn}$ configurations of $\sim$109 pm (free N-H bond: 101 pm). We conclude that the defect structures of $(NH_3)_{Zn}$ proposed in Ref. [34] have to be excluded as a model for XH_3 or XH_3^*, but other configurations of NH_3 may be involved in these complexes.

One possibility to shed light upon the chemical nature of XH_3 would be an extensive secondary ion mass spectrometry (SIMS) study. A distinct correlation between SIMS data and the XH_3 absorption strength as determined by FTIR could elucidate if the hydrogen atoms are complexed with particular impurity atoms. We performed SIMS measurements on some of our HT-grown samples and found that the nitrogen concentration was below or at the detection limit of our SIMS setup ($\approx 2 \times 10^{17}$ cm^{-3}). From the absorption strength as measured by FTIR we estimate that the XH_3 concentration of these samples is in the same order of magnitude. At the present stage, our data are insufficient to draw a decisive conclusion on the incorporation of nitrogen in XH_3.

D. The VH_3 model

An intuitive model for a defect with three equivalent O-H bonds in ZnO is the zinc vacancy decorated with three hydrogen atoms in the basal plane, $V_{Zn}H_3$. Previous works provide contradicting results on the properties of $V_{Zn}H_n$ complexes. While an early study reports that the complex with $n = 2$ has the lowest formation energy and defects with $n \geqslant 3$ are not formed [35], more recent calculations suggest that $V_{Zn}H_3$ is energetically comparable [36] or even more favorable [37] than $V_{Zn}H_2$.

Here, we present our results of first-principles calculations on $V_{Zn}H_3$. In order to validate our method we have also simulated interstitial hydrogen, H_i, and $V_{Zn}H_n$, $n = 1,2$, for comparison with previous theory and experiment. Total binding energies were calculated in reference to the zinc vacancy, V_{Zn}, and H_i in a bond-centered position, H_{BC}, according to

$$E_{bind}\left(X^q_{V_{Zn}H_n}\right) = E\left(X^q_{V_{Zn}}\right) - E(X^q) + n\left[E\left(X^q_{H_{BC}}\right) - E(X^q)\right], \tag{8}$$

where $E(X^q)$ is the total energy for the system X in charge state q. We found that both $V_{Zn}2\sigma_1^{DH}H_{BC\perp}H_{BC\parallel}$ and $V_{Zn}3H_{BC\perp}$ are stable configurations, where the latter configuration is

TABLE III. Calculated LVM frequencies of $V_{Zn}3H_{BC\perp}$ in the neutral charge state. The polarization angle is given in degrees to the c axis. Δ is the difference in the calculated and experimentally observed frequencies $\omega_{calc} - \omega_{expt.}$

Config.		Expt.	Freq. model (cm^{-1})	Δ	Pol. angle Expt. (deg.)	Pol. angle Model (deg.)
HHH	σ_2^H	3321	3346	25	0	1
HHD	σ_3^{HD}	3318	3329	11	–	24
HDD	σ_2^{HD}	3314	3313	1	–	42
HHD	σ_1^{HD}	3305	3292	–13	90	87
HHH	σ_1^H	3303	3290	–13	90	87
HHH	σ_1^H	3303	3288	–15	90	87
DDD	σ_2^D	2488	2432	–56	0	2
HDD	σ_2^{DH}	2480	2417	–63	32	26
HHD	σ_1^{DH}	2473	2406	–67	48	45
DDD	σ_1^D	2466	2398	–68	90	86
DDD	σ_1^D	2466	2393	–73	90	86
HDD	(σ_1^D)	2466	2393	–73	90	86

energetically more favorable by 0.18 eV, in qualitative agreement with the experimental findings on the XH_3 and XH_3^* complexes. It should be stressed that the gain in energy is the highest when the zinc vacancy becomes saturated with the first hydrogen to form $V_{Zn}H$ and subsequently decreases with filling more hydrogen to the complex. Hence, the actual formation of the $V_{Zn}H_3$ complex strongly depends on the number of available zinc vacancies. If zinc vacancies are abundant only $V_{Zn}H$ will exist, whereas if zinc vacancies are becoming scarce compared to the amount of isolated hydrogen atoms, complexes with a higher number of hydrogen atoms on zinc vacancies will form.

In this context, the experimentally observed differences between our HT- and VP-grown samples should be emphasized. The results of Sec. III B show that in the VP-grown samples $V_{Zn}H_2$ dominates over the XH_3 complex, while $V_{Zn}H_2$ is not observed in the HT-grown ones. A possible explanation may be differences in the relative concentration of zinc vacancies and hydrogen. Notably, our HT-grown samples contain significant amounts of Li, which can strongly influence the intrinsic point defect balance, in particular that of V_{Zn}. Consequently, the hydrogen concentration [H] in these samples may exceed $[V_{Zn}]$ much more compared to the VP-grown samples, thereby leading to the prevalence of the higher-order $V_{Zn}H_n$ complex.

The results of the vibrational mode calculations of the neutral $V_{Zn}3H_{BC\perp}$ complex are shown in Table III. For convenience of comparison the difference in the calculated and experimentally observed frequencies $\Delta = \omega_{calc} - \omega_{exp}$ is given. The vibrational frequencies in the table have been sorted according to their energy. In this presentation, it is evident that Δ decreases monotonically from the highest to the lowest modes. In particular, our calculations underestimate the D-related LVMs more than the H-related counterparts. In order to validate if this is an inherent artifact of our method we performed calculations on interstitial hydrogen in $H_{BC\parallel}$ configuration. A harmonic approximation yields a LVM frequency of 3636 cm^{-1} which is $\Delta = 25$ cm^{-1} from the well-established experimental value of 3611 cm^{-1} [3]. Δ is expected to be positive because of the error introduced through the approximation of an O-H bond potential. One way to correct this is by doing an energy scan along this mode and solving the resulting one-dimensional Schrödinger equation. We can do this under the assumption that there is no anharmonic coupling between different modes, which is a good approximation for isolated O-H bonds. This anharmonic correction yields 3444 cm^{-1} and hereby underestimates the experimental value by $\Delta = -167$ cm^{-1} although the O-H potential was now solved more accurately. Therefore our projector augmented-wave density functional method tends to underestimate vibrational energies which is, however, compensated by the overestimation from the harmonic approximation in O-H and O-D bindings. Practically this results in an error cancellation which improves the harmonic approximation. For high vibrational energies the error of the harmonic approximation dominates, whereas for lower frequencies this intrinsic error is stronger. This is illustrated by our calculated result for $D_{BC\parallel}$ with an experimental LVM of 2668 cm^{-1} where we have an offset of $\Delta = -27$ cm^{-1}. We thus conclude that although our used method introduces absolute errors we can still accurately reproduce the structure of the LVMs for a given defect. It can be seen from Table III that for the $V_{Zn}3H_{BC\perp}$ complex the experimental and calculated energy spectra are qualitatively identical. Contrary to the NH_3 model in Sec. IV C, it cannot, however, explain the observed frequency differences between hydrogen- and deuterium-related modes $\Delta\sigma^H = 24 > \Delta\sigma^D = 18$ cm^{-1}. At this stage we can neither conclusively support nor rule out $V_{Zn}H_3$ as a model for XH_3.

Our calculations predict that $V_{Zn}H_3$ is a single donor. A Bader-charge analysis shows an average charge of $0.411e$ on the hydrogen ions when the defect is in the (-1) charge state. If the defect becomes neutral this amount increases by 0.9% while the bond length only shows a minor change from 99.3 to 99.1 pm. The calculated vibrational mode of $V_{Zn}H_3$ in the ionized charge state is generally about 30–40 cm^{-1} higher in frequency than the neutral charge state.

V. SUMMARY

A hydrogen-related defect in ZnO which leads to two broad IR absorption bands at 3303 and 3321 cm^{-1} is studied by means of infrared absorption spectroscopy and first-principles theory. The combination of isotopic substitution experiments and polarization-sensitive measurements, using an extensive set of samples grown by different techniques, suggests that the absorption lines are LVMs of a defect consisting of three equivalent hydrogen atoms with the X-H bonds located in the basal plane of the defect. The experimental data rule out the previous assignment of the 3303 cm^{-1} line to a Na acceptor passivated by a single hydrogen atom. First-principles calculations for a zinc vacancy decorated with three H atoms ($V_{Zn}H_3$) produce results in agreement with the experimental observations, although the possibility that hydrogen atoms are associated with an impurity, for instance as NH_3, cannot be also excluded.

ACKNOWLEDGMENTS

This work was partially funded by the Norwegian Research Council (Norges Forskningsråd) through the FRINAT program

and the Graduate Academy of the Technische Universität Dresden. Further, the Research Council of Norway is acknowledged for the support to the Norwegian Micro- and Nano-Fabrication Facility, Nor-Fab (197411/V30) for providing essential infrastructure access. H. Haug is gratefully acknowledged for help with IR absorption measurements.

[1] G. A. Shi, M. Stavola, S. J. Pearton, M. Thieme, E. V. Lavrov, and J. Weber, Phys. Rev. B **72**, 195211 (2005).
[2] B. K. Meyer, H. Alves, D. M. Hofmann, W. Kriegseis, D. Forster, F. Bertram, J. Christen, A. Hoffmann, M. Straßburg, M. Dworzak, and U. Haboeck, Phys. Status Solidi B **241**, 231 (2004).
[3] E. V. Lavrov, F. Herklotz, and J. Weber, Phys. Rev. B **79**, 165210 (2009).
[4] F. G. Gärtner and E. Mollwo, Phys. Status Solidi B **89**, 381 (1978).
[5] E. V. Lavrov, J. Weber, F. Börrnert, C. G. Van de Walle, and R. Helbig, Phys. Rev. B **66**, 165205 (2002).
[6] E. V. Lavrov, J. Weber, and F. Börrnert, Phys. Rev. B **77**, 155209 (2008).
[7] L. E. Halliburton, L. Wang, L. Bai, N. Y. Garces, N. C. Giles, M. J. Callahan, and B. Wang, J. Appl. Phys. **96**, 7168 (2004).
[8] E. V. Lavrov, F. Börrnert, and J. Weber, Phys. Rev. B **71**, 035205 (2005).
[9] G. A. Shi, M. Stavola, and W. B. Fowler, Phys. Rev. B **73**, 081201(R) (2006).
[10] N. Parmar, M. McCluskey, and K. Lynn, J. Electron. Mater. **42**, 3426 (2013).
[11] D. Bastin, E. V. Lavrov, and J. Weber, Phys. Rev. B **83**, 195210 (2011).
[12] P. E. Blochl, Phys. Rev. B **50**, 17953 (1994).
[13] J. P. Perdew, K. Burke, and M. Ernzerhof, Phys. Rev. Lett. **77**, 3865 (1996).
[14] G. Kresse and J. Hafner, Phys. Rev. B **47**, 558 (1993).
[15] D. Karhanek, T. Bučko, and J. Hafner, J. Phys.: Condens. Matter **22**, 265006 (2010)
[16] We note that the exact relative concentration of H and D is unknown. In Fig. 2, we used the intensity ratio of the hydrogen- and the deuterium-related LVMs of the XH_3 center for a rough estimate. In Sec. IV A we will apply certain models for the microscopic structure XH_3 in order to determine r for each sample.
[17] M. D. McCluskey, S. J. Jokela, K. K. Zhuravlev, P. J. Simpson, and K. G. Lynn, Appl. Phys. Lett. **81**, 3807 (2002).
[18] F. Herklotz, E. V. Lavrov, V. Kolkovsky, J. Weber, and M. Stavola, Phys. Rev. B **82**, 115206 (2010).
[19] B. N. J. Persson and R. Ryberg, Phys. Rev. B **32**, 3586 (1985).
[20] S. G. Koch, E. V. Lavrov, and J. Weber, Phys. Rev. B **89**, 235203 (2014).
[21] K. R. Martin, P. Blaney, G. Shi, M. Stavola, and W. B. Fowler, Phys. Rev. B **73**, 235209 (2006).
[22] B. Sun, G. A. Shi, S. V. S. Nageswara Rao, M. Stavola, N. H. Tolk, S. K. Dixit, L. C. Feldman, and G. Lüpke, Phys. Rev. Lett. **96**, 035501 (2006).
[23] E. J. Spahr, L. Wen, M. Stavola, L. A. Boatner, L. C. Feldman, N. H. Tolk, and G. Lüpke, Phys. Rev. Lett. **102**, 075506 (2009).
[24] E. J. Spahr, L. Wen, M. Stavola, L. A. Boatner, L. C. Feldman, N. H. Tolk, and G. Lüpke, Phys. Rev. Lett. **104**, 205901 (2010).
[25] D. West and S. K. Estreicher, Phys. Rev. Lett. **96**, 115504 (2006).
[26] D. West and S. K. Estreicher, Phys. Rev. B **75**, 075206 (2007).
[27] E. V. Lavrov and J. Weber, Phys. Status Solidi B **243**, 2657 (2006).
[28] B. B. Nielsen, P. Johannesen, P. Stallinga, K. B. Nielsen, and J. R. Byberg, Phys. Rev. Lett. **79**, 1507 (1997).
[29] *CRC Handbook of Chemistry and Physics*, 82nd ed., edited by D. R. Lide (CRC Press LLC, Boca Raton, FL, 2001–2002).
[30] E. B. Wilson, J. C. Decius, and P. C. Cross, *Molecular Vibrations* (Dover, New York, 1980).
[31] R. S. Leigh and R. C. Newman, Semicond. Sci. Technol. **3**, 84 (1988).
[32] R. Helbig, J. Cryst. Growth **15**, 25 (1972)
[33] N. Y. Garces, N. C. Gilles, L. E. Halliburton, G. Cantwell, D. B. Eason, D. C. Reynolds, and D. C. Look, Appl. Phys. Lett. **80**, 1334 (2002).
[34] J. Bang, Y.-Y. Sun, D. West, B. K. Meyer, and S. Zhang, J. Mater. Chem. C **3**, 339 (2015).
[35] M. G. Wardle, J. P. Goss, and P. R. Briddon, Phys. Rev. B **72**, 155108 (2005).
[36] J. Koßmann and C. Hättig, Phys. Chem. Chem. Phys. **14**, 16392 (2012).
[37] S. Z. Karazhanov, E. S. Marstein, and A. Holt, J. Appl. Phys. **105**, 033712 (2009).